

Primož Peterlin

# Frequency-dependent electrodeformation of giant phospholipid vesicles in AC electric field

Received: date / Accepted: date

**Abstract** A model of vesicle electrodeformation is described which obtains a parametrized vesicle shape by minimizing the sum of the membrane bending energy and the energy due to the electric field. Both the vesicle membrane and the aqueous media inside and outside the vesicle are treated as leaky dielectrics, and the vesicle itself is modelled as a nearly spherical shape enclosed within a thin membrane. It is demonstrated (a) that the model achieves a good quantitative agreement with the experimentally determined prolate-to-oblate transition frequencies in the kHz range, and (b) that the model can explain a phase diagram of shapes of giant phospholipid vesicles with respect to two parameters: the frequency of the applied AC electric field and the ratio of the electrical conductivities of the aqueous media inside and outside the vesicle, explored in a recent paper (S. Aranda *et al.*, *Biophys. J.* 95:L19–L21, 2008). A possible use of the frequency-dependent shape transitions of phospholipid vesicles in conductometry of microliter samples is discussed.

**Keywords** electrodeformation · giant phospholipid vesicle · leaky dielectric · membrane bending energy · vesicle shape

**PACS** 87.16.D- · 41.20.Cv

## 1 Introduction

An increasing awareness of the effects of the electromagnetic field on biological samples [1], as well as its use in biotechnology [2] has instigated numerous studies

---

P. Peterlin  
University of Ljubljana, Faculty of Medicine, Institute of Biophysics,  
Lipičeva 2, SI-1000 Ljubljana, Slovenia,  
Tel.: +386-1-5437612  
Fax.: +386-1-4315127  
E-mail: primoz.peterlin@mf.uni-lj.si

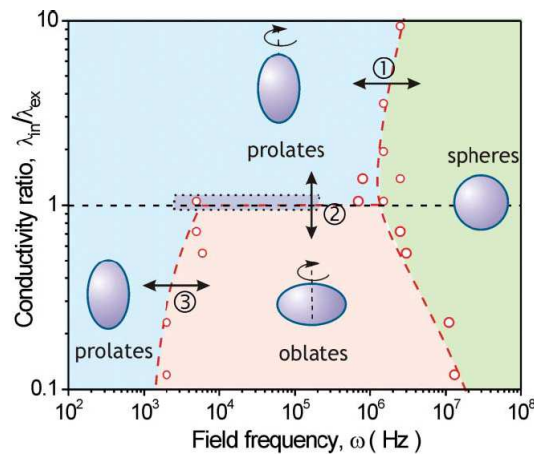


**Fig. 1** Morphological phase diagram of lipid vesicle shapes subjected to an AC electric field. The two parameters spanning the diagram are the frequency of the applied AC electric field and the ratio of the electrical conductivities of the aqueous media inside and outside the vesicle (from ref. [6]; reproduced by permission of The Royal Society of Chemistry).

on the effects of electric field on individual biological cells. When exposed to an AC electric field, biological cells exhibit several connected phenomena such as orientation, dielectrophoresis, electrorotation and deformation [3,4,5]. Of these, deformation has probably received the least attention, despite the fact that it can be conveniently studied on giant unilamellar phospholipid vesicles (GUVs) [6,7], which serve as models of biological cells.

Extensive studies of the behaviour of biological cells in the electric field have been conducted by Schwan since the 1950's [8]. However, these early studies treated cells as rigid objects. A theory of lipid bilayer elasticity [9] was needed for the first model of vesicle electrodeformation [10]. This first model predicted a prolate spheroidal deformation; this prediction was later confirmed both by improved theoretical treatments [11,12] and by experiments [13], conducted in a 2 kHz AC electric field. However, experiments where the frequency of the field was varied [14,15] have demonstrated that the vesicle shape undergoes a transition from prolate shapes at low frequencies to oblate shapes at higher frequencies. Independently, such behaviour was also predicted by Hyuga and co-workers [16,17], who described a prolate-to-oblate shape transition in certain conditions with respect to the electrical properties of the aqueous medium inside and outside the vesicle.

A recent paper [18] extended the studies of vesicle shape in electric field to higher frequencies and explored the effect of varying electrical conductivity of the internal and the external aqueous medium in a systematic manner, thus obtaining a more complex morphological phase diagram (Fig. 1). The authors have demonstrated that in the case when the conductivity of the external aqueous medium exceeds the conductivity of the aqueous medium inside the vesicle, another shape transitions exist in the MHz range in addition to the previously observed prolate-to-oblate transition in the kHz range.

The rest of this paper is structured as follows: Section 2 presents the theoretical model, which treats the vesicle as a thin shell made of leaky dielectric and derives its shape by minimizing its total energy, consisting of membrane bending energy and the energy due to the electric field. Section 3 describes the experiments investigating the prolate-to-oblate morphological shape transition in the kHz range. The results – a comparison of the model predictions with the experimental data for the prolate-to-oblate transition on the one hand and with the experimental morphological phase diagram (Fig. 1) on the other hand – are presented in Section 4. Section 5 discusses the limitations of the presented model, compares it with the existing ones, and introduces a possible application of frequency-dependent transitions of vesicle shapes for conductometry. Finally, Section 6 presents the main conclusions.

## 2 Theoretical analysis

In general, the model follows the approach introduced by Winterhalter and Helfrich [12], *i.e.*, a parametrized vesicle shape is obtained by minimizing its total free energy. Two terms enter the free energy: the membrane bending energy and the energy due to the electric field. A closed-form expression for the membrane bending energy is well-known [9], and the change of the free energy due to the electric field is calculated as the work done by the force of the electric field while deforming the vesicle [12].

Once an electric field  $\mathbf{E}$  is applied, it introduces a single distinct axis into the system, so the treatment can be limited to axially symmetric shapes. This eliminates the dependence on the longitude angle  $\phi$ , if the polar ( $z$ ) axis is chosen parallel to the applied field. Thus, the vesicle surface can be parametrized as

$$r(\theta) = s_0 + s(\theta), \quad (1)$$

where  $|s(\theta)| \ll s_0$ ,  $s_0$  denoting the deformation independent of the polar angle  $\theta$ . In an absence of deformation ( $|s(\theta)| = 0$ ),  $s_0$  equals the radius of the undeformed sphere ( $r_0$ ). The deformation is independent of the sign of the electric field and thus proportional to  $E^2$  in the lowest order. The field itself being proportional to  $\cos \theta$ , the deformation coupled with this field can be expected to be proportional to  $\cos^2 \theta$ . In terms of expansion into spherical harmonics, this limits us to a sum of even terms. Retaining only the terms proportional to  $E^2$  or lower, a quadrupolar term remains, where  $s(\theta)$  equals the second Legendre polynomial:  $s(\theta) = \frac{1}{2}s_2(3\cos^2 \theta - 1)$ , with  $s_2$  being a measure for the extent of deformation. Positive values of  $s_2$  indicate prolate deformation, while negative values indicate oblate deformation.

### 2.1 Membrane bending energy

The requirement for a local area conservation, which assures that the membrane stretching is independent of polar angle  $\theta$ , implies that a quadrupolar displacement

$\delta r_r$  in a radial direction is accompanied by a tangential displacement  $\delta r_\theta$  [12]:

$$\delta r_r = \frac{1}{2}(3 \cos^2 \theta - 1) s_2 \quad (2)$$

$$\delta r_\theta = -\cos \theta \sin \theta s_2 . \quad (3)$$

The total membrane area expansion is determined by the relationship between  $s_0$  and  $r_0$ . Taking into account the requirement for a constant vesicle volume, the following relationship for  $s_0$  is obtained:

$$s_0 = r_0 - \frac{s_2^2}{5r_0} . \quad (4)$$

The correction for a constant volume (4) contains a higher term in the powers of  $s_2$  and thus does not affect in the lowest term either the bending energy or the energy due to the electric field, yielding  $s_0 = r_0$  an adequate approximation.

The expression for the vesicle bending energy [9]:

$$G_{\text{bend}} = \frac{1}{2} k_c \oint (c_1 + c_2 - c_0)^2 dA . \quad (5)$$

Here,  $k_c$  is the bending elastic modulus of the membrane, while  $c_1$  and  $c_2$  are the principal curvatures of the membrane. The spontaneous curvature  $c_0$  vanishes for a bilayer composed of two equal layers. The integration is conducted over the total membrane area  $A$  of a quadrupolarly deformed vesicle. Up to quadratic order terms in  $s_2$ , the total bending energy of a nearly spherical vesicle can be expressed as [9]:

$$G_{\text{bend}} = 8\pi k_c + \frac{48\pi}{5} k_c \left( \frac{s_2}{r_0} \right)^2 . \quad (6)$$

This can be readily interpreted as the bending energy of a sphere plus an addition due to the quadrupolar deformation.

## 2.2 Contribution of the electric field

The first step in evaluating the contribution of the electric field to the total free energy is calculating the electric field. The present treatment is limited to small deviations of vesicle shape from the sphere, which greatly simplifies the treatment: instead of computing the electric field in the presence of the actual vesicle shape, one can compute the electric field in the presence of a spherical shell. Both the aqueous solution inside and outside the vesicle and the vesicle membrane are treated as lossy dielectrics. The aqueous solutions inside and outside the vesicle usually have identical dielectric permittivity, while their electrical conductivities can differ (Fig. 2).

In order to compute the forces exerted by the electric field on the vesicle, one first has to compute the electric field around a vesicle. Gauss' law  $\nabla \cdot \mathbf{D} = 0$  together with the requirement for an irrotational electric field  $\nabla \times \mathbf{E} = 0$ , which stems from Faraday's law for electromagnetic induction, yields the Laplace equation for the electric potential  $U$  [19]:

$$\nabla^2 U = 0 . \quad (7)$$

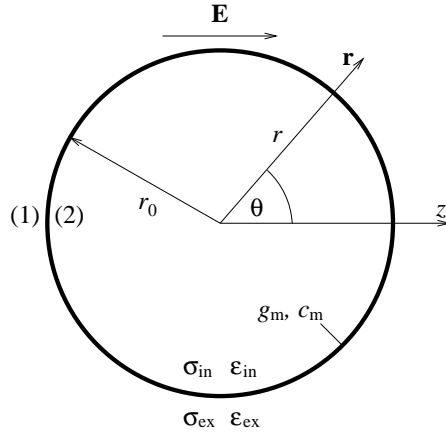


**Fig. 2** A vesicle is modelled in spherical coordinates  $(r, \theta)$  as a spherical shell with a radius  $r$  exposed to an external electric field  $\mathbf{E}$ . The conductivity and permittivity of the aqueous solution outside are denoted by  $\sigma_{\text{ex}}$  and  $\epsilon_{\text{ex}}$ , and the corresponding quantities in the vesicle interior by  $\sigma_{\text{in}}$  and  $\epsilon_{\text{in}}$ . Membrane surface transconductance and surface capacitance are denoted by  $g_m$  and  $c_m$ , respectively.

The boundary conditions on the membrane ( $r = r_0$ ) require that the total surface charge density, including both free charge and displacement charge, must vanish. The case where a finite potential can be supported across the membrane is known as the series admittance limit ([3], pp. 230-232). In the spherical geometry, this yields a system of equations

$$(\sigma_{\text{ex}} - i\omega\epsilon_{\text{ex}})E_r^{(1)}(r_0) = (\sigma_{\text{in}} - i\omega\epsilon_{\text{in}})E_r^{(2)}(r_0), \quad (8)$$

$$(\sigma_{\text{ex}} - i\omega\epsilon_{\text{ex}})E_r^{(1)}(r_0) = (g_m - i\omega c_m) \left( U^{(2)}(r_0) - U^{(1)}(r_0) \right). \quad (9)$$

Apart from (8) and (9), the system is constrained by two additional conditions: one requiring that the electric field far away from the vesicle is unperturbed, and the other requiring that the electric field is finite inside the vesicle. Membrane surface transconductance  $g_m$  and surface capacitance  $c_m$  are related to membrane electric conductivity and dielectric permittivity:  $g_m = \sigma_m/h$  and  $c_m = \epsilon_m/h$ ,  $h$  being the membrane thickness.

In spherical coordinates, (7) readily decouples into the radial and the angular part, and can be solved with the usual ansatz:

$$U^{(k)} = \frac{1}{2} \left[ \left( a^{(k)} r + \frac{b^{(k)}}{r^2} \right) \cos \theta e^{-i\omega t} + \text{C.C.} \right]. \quad (10)$$

The coefficients  $a^{(k)}, b^{(k)}$ ;  $k = 1, 2$ , which can in general be complex to allow for a phase shift, are determined from the boundary conditions (8,9).

The conditions for an unperturbed field far away from the vesicle and a finite field inside the vesicle immediately yield two coefficients:

$$a^{(1)} = -E_0, \quad (11)$$

$$b^{(2)} = 0. \quad (12)$$

The two remaining coefficients are obtained by solving (8,9):

$$a^{(2)} = -\frac{3E_0 r}{\Delta} \left[ (g_m - i\omega c_m)(\sigma_{\text{ex}} - i\omega \varepsilon_{\text{ex}}) \right], \quad (13)$$

$$b^{(1)} = -\frac{E_0 r^3}{\Delta} \left[ \sigma_{\text{ex}} \sigma_{\text{in}} + g_m r (\sigma_{\text{ex}} - \sigma_{\text{in}}) - (\varepsilon_{\text{ex}} \varepsilon_{\text{in}} + c_m r (\varepsilon_{\text{ex}} - \varepsilon_{\text{in}})) \omega^2 \right. \\ \left. - i(g_m r (\varepsilon_{\text{ex}} - \varepsilon_{\text{in}}) + c_m r (\sigma_{\text{ex}} - \sigma_{\text{in}}) + \varepsilon_{\text{in}} \sigma_{\text{ex}} + \varepsilon_{\text{ex}} \sigma_{\text{in}}) \omega \right], \quad (14)$$

$$\Delta = 2\sigma_{\text{ex}} \sigma_{\text{in}} + g_m r (2\sigma_{\text{ex}} + \sigma_{\text{in}}) - (2\varepsilon_{\text{ex}} \varepsilon_{\text{in}} + c_m r (2\varepsilon_{\text{ex}} + \varepsilon_{\text{in}})) \omega^2 \\ - i(g_m r (2\varepsilon_{\text{ex}} + \varepsilon_{\text{in}}) + c_m r (2\sigma_{\text{ex}} + \sigma_{\text{in}}) + 2(\varepsilon_{\text{in}} \sigma_{\text{ex}} + \varepsilon_{\text{ex}} \sigma_{\text{in}})) \omega. \quad (15)$$

The surface density of the forces exerted on the boundary of dielectrics by the electric field can be computed as a scalar product of the Maxwell stress tensor and a vector normal to the membrane:

$$\mathbf{f} = (\underline{\mathbf{T}}^{(1)} - \underline{\mathbf{T}}^{(2)}) \mathbf{e}_r. \quad (16)$$

The force vanishes in a homogeneous medium, but can in general be non-zero on the boundaries of media with different electrical properties. The Maxwell stress tensor is defined as

$$\underline{\mathbf{T}} = \mathbf{D} \otimes \mathbf{E} - \frac{1}{2} (\mathbf{D} \cdot \mathbf{E}) \underline{\mathbf{I}}, \quad (17)$$

where  $\underline{\mathbf{I}}$  denotes the identity matrix.

Unlike in the case of the bending energy term (6), for which a closed-form expression was obtained, an approach where energy difference is computed is employed here.  $\delta G_{\text{field}}$  denotes a small change in the energy due to the electric field, when a sphere ( $s_2 = 0$ ) is perturbed by a small deformation change  $\delta s_2$ . This energy difference is calculated as the work done by the forces of the electric field during the displacement of membrane elements  $\delta \mathbf{r}$  (equations 2,3), integrated over the entire membrane area [12]:

$$\delta G_{\text{field}} = - \oint (\mathbf{f} \cdot \delta \mathbf{r}) dA. \quad (18)$$

The integration is conducted over a sphere, which is consistent with the limit of small deformations ( $s_2 \ll r_0$ ).

Substituting the coefficients (11–15) into (18) yields a lengthy expression for  $\delta G_{\text{field}}$ , which can be written as a sum of two dispersion terms:

$$\delta G_{\text{field}} = -\frac{6\pi}{5} \varepsilon_w E_0^2 r_{\text{out}}^2 s_2 \left( \xi_{\infty} + \frac{\xi_1}{1 + \omega^2 \tau_1^2} + \frac{\xi_2}{1 + \omega^2 \tau_2^2} \right). \quad (19)$$

Three dimensionless coefficients  $\xi_{\infty}$ ,  $\xi_1$ , and  $\xi_2$ , and two characteristic times  $\tau_1$  and  $\tau_2$  are rather lengthy expressions involving six different material constants:  $\varepsilon_{\text{ex}}$ ,  $\varepsilon_{\text{in}}$ ,  $\sigma_{\text{ex}}$ ,  $\sigma_{\text{in}}$ ,  $c_m$ ,  $g_m$ , and the vesicle radius  $r_0$ .

### 2.3 Vesicle deformation

For small deformations, quadrupolar deformation only induces small perturbative changes in the vesicle bending energy and the energy due to the electric field.

$$G_{\text{bend}}(s_2) \approx G_{\text{bend}}(s_2 = 0) + \frac{1}{2} \left. \frac{\partial^2 G_{\text{bend}}}{\partial s_2^2} \right|_{s_2=0} s_2^2 \quad (20)$$

$$G_{\text{field}}(s_2) \approx G_{\text{field}}(s_2 = 0) + \left. \frac{\partial G_{\text{field}}}{\partial s_2} \right|_{s_2=0} s_2 \quad (21)$$

Even though the total energy of the vesicle formally depends on two parameters,  $r_0$  and  $s_2$ , the constraint requiring a constant vesicle volume eliminates one degree of freedom, thus yielding (20–21). It is also worth noting that the fact that neither prolate ( $s_2 > 0$ ) nor oblate shapes ( $s_2 < 0$ ) have a bending energy lower than those of a sphere means that the expansion for the bending energy (20) contains no linear term.

Equilibrium vesicle deformation, expressed in terms of  $s_2$ , can then be calculated by minimizing the total free energy over  $s_2$ :

$$\frac{d}{ds_2} (G_{\text{bend}} + G_{\text{field}}) = 0. \quad (22)$$

Expressing the equilibrium vesicle deformation  $s_2$  from (22) at given conditions yields:

$$s_2 = \frac{1}{16} \frac{r_0^4 \epsilon_w E_0^2}{k_c} \left( \xi_\infty + \frac{\xi_1}{1 + \omega^2 \tau_1^2} + \frac{\xi_2}{1 + \omega^2 \tau_2^2} \right). \quad (23)$$

As one can see, the dependence of vesicle deformation  $s_2$  on the angular frequency  $\omega = 2\pi\nu$  contains two dispersion terms. It is worth emphasizing that the only approximation used in deriving the expression (23) is that of a small deformation ( $s_2 \ll r_0$ ). Also worth noting is the fact that the only parameter related to membrane elasticity,  $k_c$ , only scales  $s_2$ ; frequency-dependent electrodeformation of vesicles is entirely governed by the electrical parameters of the membrane and the aqueous medium and by the vesicle size.

Fig. 3 shows vesicle deformation in dependence of the angular frequency  $\omega$  of the applied AC electric field. Its most prominent feature is that the deformation exhibits a prolate-to-oblate transition at  $\omega \sim 10^4$  Hz (*i.e.*,  $\nu \sim 10^3$  Hz) in the case when  $\sigma_{\text{in}} < \sigma_{\text{ex}}$  (*e.g.*,  $\sigma_{\text{in}} = 0.8 \sigma_{\text{ex}}$ , solid curve). On the other hand, vesicle shape remains prolate up to  $\omega \sim 10^7$  Hz ( $\nu \sim 10^6$  Hz) when  $\sigma_{\text{in}} > \sigma_{\text{ex}}$  (*e.g.*,  $\sigma_{\text{in}} = 1.3 \sigma_{\text{ex}}$ , coarsely dashed curve). In both cases, a transition to spherical shape ( $s_2 \approx 0$ ) is observed at  $\omega \sim 10^7$  Hz ( $\nu \sim 10^6$  Hz). All these features are in agreement with the experimental findings [18]. The transition to spherical shape, however, occurs as low as  $\omega \sim 10^4$  Hz when the conductivities inside and outside are equal,  $\sigma_{\text{in}} = \sigma_{\text{ex}}$  (Fig. 3, finely dashed curve). Some of the points in Fig. 1 around  $\sigma_{\text{in}}/\sigma_{\text{ex}} = 1$  may indicate that such transitions have also been observed. It needs to be pointed out, however, that this is not a distinguished property of the  $\sigma_{\text{in}} = \sigma_{\text{ex}}$  case, but merely a coincidence at given values of material properties and at given vesicle size.

The lengthy expressions for the coefficients  $\xi_\infty$ ,  $\xi_1$ ,  $\xi_2$ ,  $\tau_1$  and  $\tau_2$  figuring in (23) can be somewhat simplified. First of all, it is reasonable to assume that the

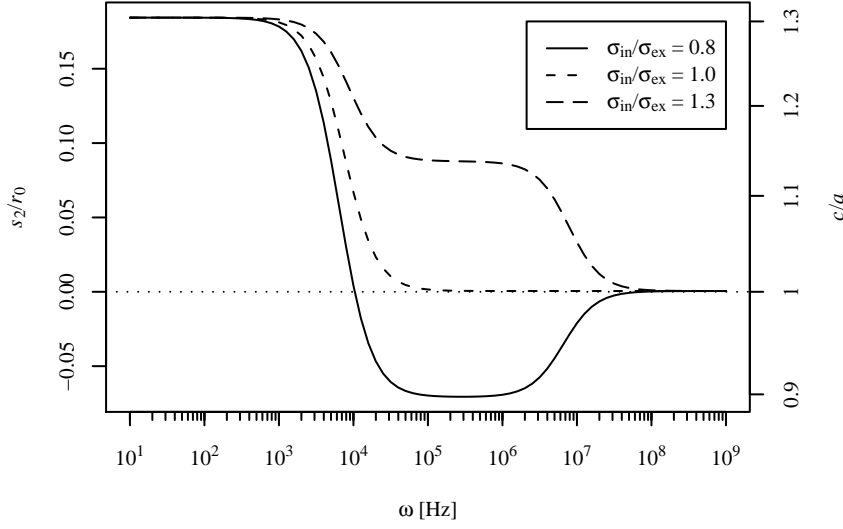


**Fig. 3** Vesicle deformation as a function of the frequency  $\omega = 2\pi\nu$  of the applied AC electric field. Vesicle deformation is shown both in terms of quadrupolar deformation  $s_2$  normalized to  $r_0$  (primary y-axis, left) and vesicle semi-axes ratio  $c/a \approx (r_0 + s_2)/(r_0 - s_2/2)$  (secondary y-axis, right). The three curves were computed for three different ratios between the electrical conductivity of the external aqueous medium and the electrical conductivity of the internal aqueous medium. The dotted line separates prolate shapes from oblate ones. Other parameters used for computation were  $r_0 = 20 \mu\text{m}$ ,  $\sigma_{\text{ex}} = 50 \mu\text{S/cm}$ ,  $\sigma_{\text{m}} = 10^{-14} \text{ S/m}$ ,  $\epsilon_{\text{w}} = 80\epsilon_0$ ,  $\epsilon_{\text{m}} = 2.5\epsilon_0$ ,  $h = 4 \text{ nm}$ ,  $k_{\text{c}} = 1.2 \times 10^{-19} \text{ J}$ ,  $E_0 = 500 \text{ V/m}$ .

dielectric permittivity of the aqueous medium inside the vesicle does not differ significantly from the dielectric permittivity of the external medium,  $\epsilon_{\text{ex}} = \epsilon_{\text{in}} \equiv \epsilon_{\text{w}}$  (this is an approximation; it is known that the dielectric permittivity of water decreases with the increasing concentration of salt in it; *e.g.*, the dielectric permittivity of physiological saline is only  $\approx 72 \epsilon_0$ , [20]). A further simplification is possible in the case when realistic values for material parameters are taken into account: (a) the conductivity of the aqueous solution greatly exceeds that of the membrane,  $\sigma_{\text{w}} \gg \sigma_{\text{m}}$ , and (b) with  $\epsilon_{\text{w}} \approx 80\epsilon_0$ ,  $\epsilon_{\text{m}} \approx 2.5\epsilon_0$ , and  $r_0/h \sim 1000$ , then  $\epsilon_{\text{w}} \ll (r_0/h)\epsilon_{\text{m}}$ . Retaining only the largest terms, one obtains:

$$\xi_{\infty} \approx \frac{\epsilon_{\text{w}}(4r_0c_{\text{m}} + \epsilon_{\text{w}})}{(3r_0c_{\text{m}} + 2\epsilon_{\text{w}})^2}, \quad (24)$$

$$\tau_1 \approx \frac{\epsilon_{\text{w}}}{\sigma_{\text{ex}}} \frac{3}{2+x}, \quad (25)$$

$$\tau_2 \approx \frac{r_0c_{\text{m}}}{\sigma_{\text{ex}}} \frac{2+x}{2x}. \quad (26)$$

Here,  $x = \sigma_{\text{in}}/\sigma_{\text{ex}}$  has been introduced for the ratio of the conductivities of the aqueous medium inside and outside the vesicle.



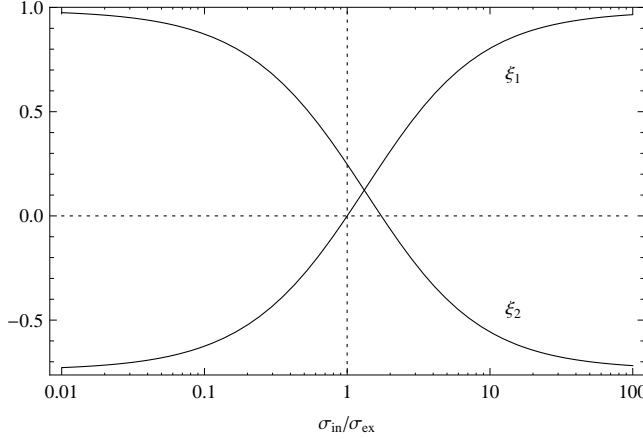


**Fig. 4** The coefficients  $\xi_1$  and  $\xi_2$  figuring in (23) plotted for different values of the ratio of the internal and the external electrical conductivity,  $x = \sigma_{\text{in}}/\sigma_{\text{ex}}$ . Other parameter values used for computation were the same as in Fig. 3.

The two characteristic times are related to two distinct physical processes:  $\tau_1$  is the relaxation time for the Maxwell-Wagner interfacial polarization, and  $\tau_2$  is the charging time of a spherical capacitor. In the literature (see, *e.g.*, [21, 16, 22, 3]) the expressions for them are often encountered in a slightly more general form, which distinguishes between the dielectric permittivity of the internal and the external aqueous medium.

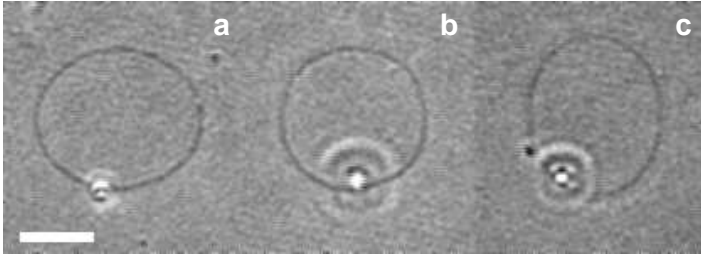
As expected,  $\xi_\infty$  does not depend on conductivities, and the curves for different  $\sigma_{\text{in}}/\sigma_{\text{ex}}$  plotted in Fig. 3 merge into a single one at  $\omega \rightarrow \infty$ . One can also see that in the high-frequency limit, the deformation is always slightly prolate,  $\xi_\infty \approx (h/r_0)(\epsilon_w/\epsilon_m) \lesssim 0.01$ . Such subtle deformation is however in reality likely to be subdued by the thermal fluctuations, and is therefore difficult to detect experimentally.

Fig. 4 shows how the coefficients  $\xi_1$  and  $\xi_2$  change when the ratio of the internal and the external electrical conductivity  $x = \sigma_{\text{in}}/\sigma_{\text{ex}}$  is varied within two decades at given values of material parameters. On the interval  $x \in [1/100, 100]$ ,  $\xi_1$  and  $\xi_2$  can be approximated by rational functions of  $x$ :

$$\xi_1 \approx -\frac{(r_o c_m + \epsilon_w)(3r_0 c_m + 4\epsilon_w) + (r_o c_m + \epsilon_w)(3r_0 c_m + 4\epsilon_w)x}{4(r_0^2 c_m^2 + 5r_o c_m \epsilon_w + 4\epsilon_w^2) + (3r_0^2 c_m^2 + 13r_o c_m \epsilon_w + 12\epsilon_w^2)x}, \quad (27)$$

$$\xi_2 \approx \frac{16(r_0^2 c_m^2 + 3r_o c_m \epsilon_w + 2\epsilon_w^2) - (9r_0^2 c_m^2 + 15r_o c_m \epsilon_w + 4\epsilon_w^2)x}{4(3r_0^2 c_m^2 + 13r_o c_m \epsilon_w + 4\epsilon_w^2) + 4(4r_0^2 c_m^2 + 20r_o c_m \epsilon_w + 24\epsilon_w^2)x}. \quad (28)$$

It is possible to derive an approximate expression for the critical value of  $x$ , below which the prolate-to-oblate transition occurs. In the intermediate region,  $1/\tau_2 < \omega < 1/\tau_1$ , the function  $\xi(\omega; x) = \xi_\infty + \xi_1/(1 + \omega^2 \tau_1^2) + \xi_2/(1 + \omega^2 \tau_2^2)$  figuring in (23) approximately evaluates to  $\xi(\omega; x) \approx \xi_\infty + \xi_1$ . This needs to be negative in order for an oblate deformation. From this requirement, an approxi-



**Fig. 5** Phase-contrast micrograph of a vesicle in an AC electric field in response to the frequency of the applied field: (a) 1 kHz, (b) 11 kHz, (c) 29 kHz. The direction of the electric field corresponds to the horizontal direction. The bar represents 10  $\mu\text{m}$ . The conductivity of the aqueous medium is  $\sigma_m = 17 \mu\text{S/cm}$ .

mate expression for  $x_{\text{crit}}$  can be obtained:

$$x_{\text{crit}} \approx \frac{27 r_0 c_m + 93 \epsilon_w}{27 r_0 c_m + 111 \epsilon_w}. \quad (29)$$

Substituting realistic values for material parameters and vesicle size into (29), one finds that  $x_{\text{crit}} \approx 0.97$  for a vesicle with  $r_0 = 5 \mu\text{m}$ ,  $x_{\text{crit}} \approx 0.986$  for a vesicle with  $r_0 = 10 \mu\text{m}$ , and  $x_{\text{crit}} \approx 0.997$  for a vesicle with  $r_0 = 50 \mu\text{m}$ .

### 3 Experiment

#### 3.1 Vesicle preparation

Giant unilamellar vesicles (GUVs) were prepared from commercially available (Avanti Polar Lipids, Alabaster, AL, USA) synthetic 1-palmitoyl-2-oleoyl-*sn*-glycero-3-phosphocholine (POPC) in double-distilled water using the electroformation method [23,24] in a chamber which allows for an easy access of the resulting vesicle suspension [25]. In order to alter the conductivity of the solution, sodium chloride was added to the solution in concentration of up to  $0.2 \times 10^{-3} \text{ mol/L}$ .

#### 3.2 Experimental procedure

The experimental chamber consisted of two 0.1 mm thick stainless steel electrodes mounted on an object glass, leaving a 0.6 mm wide gap between the electrodes. The cover slip was mounted with vacuum grease (Baysilone; Bayer, Leverkusen, Germany), enclosing a few drops of vesicle suspension. The chamber was placed onto an inverted light microscope (Zeiss/Opton IM 35, objective Zeiss Ph2 Plan 40/0.60; Zeiss, Oberkochen, Germany), and phase contrast technique was used. The micrograph was recorded using a CCD camera (Cohu 6700; Cohu, San Diego, USA), taped using a U-Matic VCR (Sony VO-9800P) and later digitized on a PC with a frame grabber (Matrox Meteor II; Matrox, Dorval, Canada). The same computer was used to set the voltage and frequency of the applied electric field, driving a GPIB-controlled function generator (Iskra MA-3735; Iskra, Horjul, Slovenia).

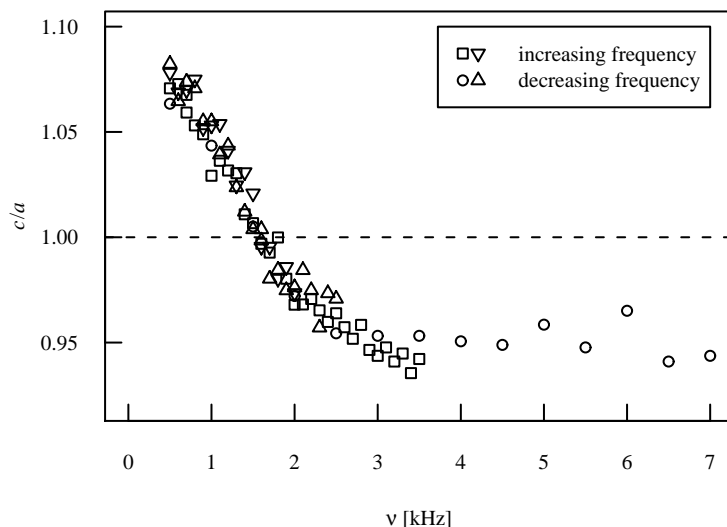


**Fig. 6** Prolate-to-oblate transition of a phospholipid vesicle in the kHz range. Vesicle deformation is expressed as the ratio of its semi-axis in the direction along the field ( $c$ ) and its semi-axis perpendicular to the field ( $a$ ). Vesicle radius  $r_0 = 19.8 \pm 0.1 \mu\text{m}$ , conductivity of the aqueous medium  $\sigma_{\text{in}} = 4.6 \mu\text{S/cm}$ .

Using an acoustic coupler connected to RS-233 port and a telephone handset with an audio jack, the data about the selected voltage and frequency were simultaneously recorded onto one audio channel, while the other audio channel was left for the experimentalist's comments during the course of experiment [26].

In the experiment, the prolate-to-oblate transition frequency for a given vesicle was first coarsely estimated by testing the effect of the electric field at 2–3 different frequencies. After this coarse estimate, a programmed sequence of step-wise frequency change was applied. The frequency step ranged from 100 Hz to 1 kHz, depending on the vesicle, and the duration of the step was approximately 3 s. This duration was experimentally selected as being long enough for the vesicle to adapt to a small frequency change, yet short enough to minimize dielectrophoretic drift and allow repetitive measurements. The programmed sequence was repeated several times with increasing and decreasing frequencies in order to observe possible hysteresis (Fig. 6). To allow a more precise determination of transition frequency, the range was narrowed and the frequency steps were decreased in the later runs (symbols  $\square$ ,  $\triangle$ , and  $\nabla$  in Fig. 6).

## 4 Results

### 4.1 Analysis of the experimental data

A total of 46 vesicle recordings were examined. After discarding the recordings with a vesicle relative volume too close to 1, where no noticeable shape change

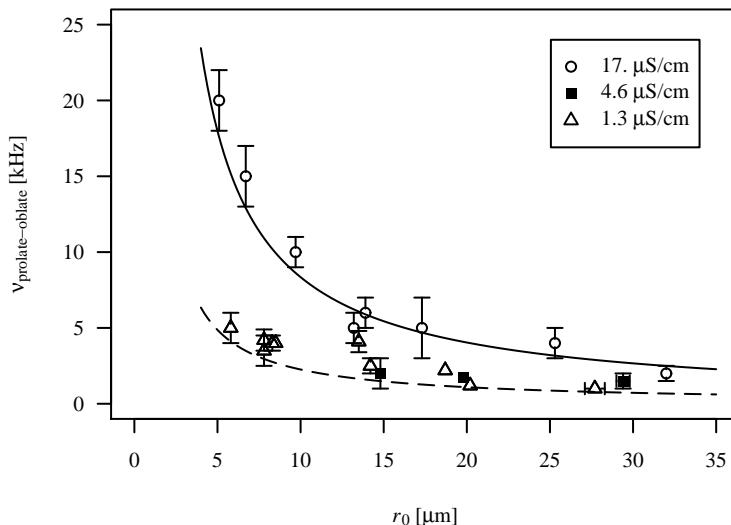


**Fig. 7** The dependence of the prolate-to-oblate transition frequency on the vesicle size and the conductivity of the aqueous medium. Three runs of experiments with three different conductivities of the aqueous medium were performed: 17, 4.6, and 1.3  $\mu\text{S/cm}$ . The solid line corresponds to numerically solving  $s_2 = 0$  (Eq. 23) for  $\omega$ , with  $\sigma_{\text{in}} = 17 \mu\text{m}$ , and the dashed line with  $\sigma_{\text{in}} = 4.6 \mu\text{m}$ . In both cases,  $\sigma_{\text{in}}/\sigma_{\text{ex}} = 0.9$ . Other parameter values used for computation were the same as in Fig. 3.

was observed, as well as the recordings in which the experiment was interrupted by the dielectrophoretic drift of a vesicle to a region where further observations were not possible, 21 measurements on different vesicles were taken into consideration for analysis. Of these, 8 were prepared in a medium with conductivity 17  $\mu\text{S/cm}$ , 3 in a medium with conductivity 4.6  $\mu\text{S/cm}$  and 10 in a medium with conductivity 1.3  $\mu\text{S/cm}$ . The transition frequency for the prolate-to-oblate transition vs. vesicle size is plotted in Fig. 7. Transition frequencies are reciprocally related to the vesicle radius, which is consistent with the recently published findings of another group (K. Antonova *et al.*, in press).

The existence of prolate-to-oblate transitions indicates that the ratio  $\sigma_{\text{in}}/\sigma_{\text{ex}}$  in the experiments was below  $x_{\text{crit}}$ , even though the compositions of the aqueous solution in the vesicle interior and the vesicle exterior were initially identical. We would like to propose an explanation for this phenomenon. First, we need to emphasize that the conductometer electrode we used requires at least 6 ml of sample, therefore it was impossible to measure directly the conductivity of the vesicle solution. Instead, the conductivity of the aqueous medium was measured before it was used for hydrating the phospholipid film. The conductivity of the aqueous solution may increase afterwards by the impurities introduced either at the electroformation process, during storage or during sample preparation. In order to test this hypothesis, we performed a separate experiment, where we simulated the manipulation of a vesicle sample. Two flasks were filled with 0.03 mmol/L solution of NaCl in 0.1 mol/L sucrose solution ( $\sigma = 14.5 \mu\text{S/cm}$ ). The first flask was kept

sealed in cold storage during the course of the experiment, while the second flask was brought to room temperature every day, and a small amount of the solution was pipetted out for conductivity measurement before returning the flask back to cold storage. While the conductivity of the solution in the first flask remained unchanged, the conductivity of the solution in the second flask increased by  $\approx 8\%$  with each consecutive pipetting, reaching  $31.5 \mu\text{S}/\text{cm}$  after 11 days. We can presume that similar processes occur in vesicle suspension, where the conductivity of the solution in the vesicle interior remains unchanged as the phospholipid membrane is virtually impermeable for ions, while the conductivity of the solution in the vesicle exterior increases with each successive pipetting. Since even for the smallest of the vesicles shown in Fig. 7 ( $r_0 \approx 5 \mu\text{m}$ ),  $x_{\text{crit}} \approx 0.97$  (cf. Eq. 29), it is clear that at such low conductivities of the solution, an 8% increase of the conductivity of the external medium caused by a single pipetting is sufficient to bring the vesicle suspension into the regime where oblate shapes exist in the intermediate frequency range.

The two computed lines in Fig. 7 were obtained by numerical root-finding of  $s_2 = 0$ ,  $s_2$  being defined by (23). The initial conductivity of the solution ( $17 \mu\text{S}/\text{cm}$  and  $4.6 \mu\text{S}/\text{cm}$ , respectively) was taken as the conductivity of the internal aqueous medium, while the conductivity of the external aqueous medium is  $1/0.9 \sigma_{\text{in}}$ , or approximately 10% higher. The quantitative agreement with the measured data at  $17 \mu\text{S}/\text{cm}$  and  $4.6 \mu\text{S}/\text{cm}$  is within the experimental error, while the data for  $1.3 \mu\text{S}/\text{cm}$  coincide with those for  $4.6 \mu\text{S}/\text{cm}$ . This may indicate that the actual electrical conductivity  $\sigma_{\text{in}}$  in this latter case was not  $1.3 \mu\text{S}/\text{cm}$ , but somewhat higher (estimated around  $5 \mu\text{S}/\text{cm}$ ).

## 4.2 Morphological diagram

In order to plot a morphological phase diagram akin to the one shown in Fig. 1, two distinct regimes have to be considered. For  $\sigma_{\text{in}}/\sigma_{\text{ex}} < 1$ , vesicle deformation  $s_2$  (23) changes sign, and the prolate-to-oblate and the oblate-to-spherical transitions can be computed by solving  $s_2 = 0$  numerically. For  $\sigma_{\text{in}}/\sigma_{\text{ex}} > 1$ ,  $s_2$  remains positive, and instead one has to rely on the characteristic times (25, 26). Here, the relaxation term containing  $\tau_1$  corresponds to prolate-to-spherical transition in Fig. 1. The relaxation term corresponding to  $\tau_2$  corresponds to an unobserved transition, *i.e.*, a prolate vesicle is expected to become slightly less prolate (see also the dashed curve in Fig. 3) at frequencies  $\omega \gtrsim 1/\tau_2$ . Such subtle changes, however, are probably difficult to quantify experimentally, and have therefore not been reported in [18].

The results, shown in Fig. 8, show a reasonable agreement with the experimental diagram (Fig. 1). In particular, for  $\sigma_{\text{in}} < \sigma_{\text{ex}}$ , the prolate-to-oblate transition frequency increases with increasing  $\sigma_{\text{in}}/\sigma_{\text{ex}}$ . The prolate-to-spherical transition for  $\sigma_{\text{in}} > \sigma_{\text{ex}}$  also increases with increasing  $\sigma_{\text{in}}/\sigma_{\text{ex}}$ , while the oblate-to-spherical transition, observed for  $\sigma_{\text{in}} < \sigma_{\text{ex}}$ , decreases with increasing  $\sigma_{\text{in}}/\sigma_{\text{ex}}$ . All these observations are in agreement with the experiment.

We would also like to comment on the reported coexistence of prolate and oblate vesicle shapes at  $x \approx 1$  in the intermediate frequency range [18]. As we have shown earlier (Fig. 7), the prolate-to-oblate transition frequency exhibits a strong dependence on vesicle size: the transition frequency for a fairly large

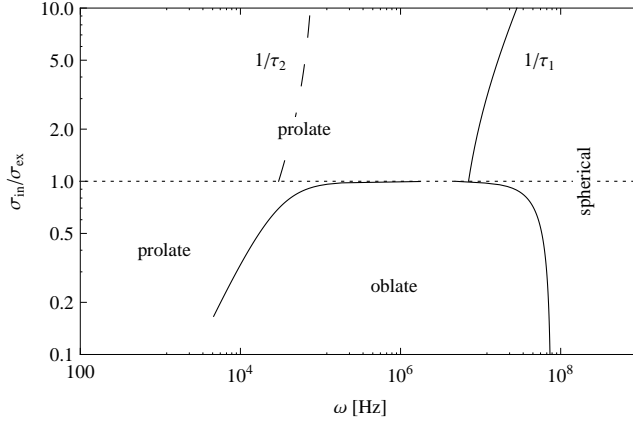


**Fig. 8** Prolate and oblate vesicle deformation plotted for different values of the ratio of the internal and the external electrical conductivity,  $x = \sigma_{in}/\sigma_{ex}$ . In the  $x < 1$  region, the sign changes in (23), and either prolate-to-oblate transition or oblate-to-spherical transitions are computed, while for  $x > 1$ , reciprocal characteristic times  $1/\tau_1$  and  $1/\tau_2$  are plotted. Other parameter values used in evaluation were the same as in Fig. 3. The dashed curve corresponds to the relaxation which does not manifest itself as a morphological shape transition.

vesicle ( $r_0 = 50 \mu\text{m}$ ) is  $\nu_2 \approx 3 \text{ kHz}$ , while for a small vesicle ( $r_0 = 5 \mu\text{m}$ ) it is  $\nu_2 \approx 30 \text{ kHz}$ . Within this frequency interval, it is thus quite feasible to observe a small prolate vesicle simultaneously with a large oblate vesicle. While the authors do not comment on the relative sizes of the vesicles in question, we believe this phenomenon can be explained if: (a) the  $\sigma_{in}/\sigma_{ex}$  ratio was below  $x_{crit}$  (*i.e.*, slightly below 1), thus making oblate shapes possible in the intermediate frequency range, and (b) the frequency was above the prolate-to-oblate transition frequency for the larger vesicle and below the prolate-to-oblate transition frequency for the smaller vesicle.

## 5 Discussion

### 5.1 Comparison with earlier results

While the model presented above builds on the legacy of the model developed over 20 years ago by Winterhalter and Helfrich [12], it departs from it in two aspects. Firstly, it allows for a different electric conductivity in the vesicle interior and the vesicle surroundings, and secondly, it is simplified by treating the vesicle membrane as a thin shell right from the start. The first modification was a necessity imposed by the experiments presented in [18]. The limitation to thin shells is appropriate since any results applicable to giant vesicles fall into this limit ( $\gamma \approx 1$  in [12]). The results presented here thus do not differ significantly from those obtained by the authors who started from a general finite-thickness model (T. Yamamoto *et al.*, to appear). Treating membrane thickness as finite is, however, always required when one attempts to tackle membrane dielectric anisotropy [27,28,29,30,31].

Hyuga *et al.* [16] provide treatment both for the vesicle deformation in an AC electric field and the response of the vesicle to a step-wise change in  $E$ , and arrive at the expressions (25, 26). However, they later conclude that the fast mode dampens very quickly and that only the effects of the slow mode are expected to show a visible influence on deformation dynamics, and consequently focus on the lower (*i.e.*, prolate-to-oblate) transition.

More recently, a theoretical analysis of the experimental results presented in [18] has been published by the same group [32], where a force-balance approach is used instead of energy minimization. While this does not introduce any major advantage in the problems treated here, *i.e.*, the phase diagram of vesicle shapes, it allowed a more correct prediction of not only the nature of deformation, but also of its extent (see below). Even more important, by extending the treatment beyond the equilibrium shape it opens a possibility of treating vesicle dynamics.

Finally, we find it necessary to relate the results in this paper with our own earlier results [31], where we argued that the prolate-to-oblate transition can be explained by the dielectric anisotropy of the membrane. In view of later experimental findings [18], which put the prolate-to-oblate transition into a broader context, as well as of the fact that even a very minute difference in the electrical conductivities of the aqueous medium inside and outside the vesicle (*cf.* eq. 29) makes prolate-to-oblate transition possible, we believe it is quite possible that the observed prolate-to-oblate transition was caused primarily by a minute unintended increase of the conductivity of the external aqueous medium, which may have overshadowed other possible effects. Even though the frequency-dependent electrodeformation of giant vesicles is likely to be primarily governed by other effects, we however continue to believe that the dielectric anisotropy of the phospholipid membrane is a phenomenon worth investigating.

## 5.2 Quantitative estimate of vesicle deformation

Though simple, the model presented in this paper provides a fairly accurate description of the experimentally obtained morphological phase diagram (Fig. 1), *i.e.*, it predicts the nature of deformation (prolate, oblate, or spherical), and the frequencies at which the transitions between these shapes occur. However, being limited by design to deformations close to spherical, this model, like the original Winterhalter-Helfrich model, does not predict the extent of deformation correctly. In the case of the Winterhalter-Helfrich model, this feature has already been noted [18, 32]. For the most part, the extent of deformation is determined by the relative volume of the vesicle, *i.e.*, a flaccid vesicle deforms more than a nearly spherical one. For simplicity, the treatment presented in this paper omits the effects of thermal fluctuations, which have already been treated elsewhere [33, 34].

## 5.3 Application in microliter conductometry

A quantitative model of vesicle shape with respect to the electrical conductivity of the medium inside and outside the vesicle allows us to exploit this phenomenon from the other end: a vesicle with a known internal conductivity and a measurable size can serve as a probe for sensing the electrical conductivity of the medium

in its surroundings. For this potential application, the kHz-range prolate-to-oblate transition seems particularly well-suited, because (a) it is an easily observable qualitative change in the vesicle shape which occurs in a narrow frequency interval, and (b) the transition frequency exhibits a strong dependence on vesicle size, which allows for some tuning, *i.e.*, in a heterogeneous vesicle population, one can select the vesicle which manifests the effect most prominently. Recent developments in vesicle preparation methods [35,36] also bring the physiological conductivities into reach.

## 6 Conclusions

It has been demonstrated that a modified Winterhalter-Helfrich model [12] which obtains a parametrized vesicle shape by minimizing the sum of the membrane bending energy and the energy due to the electric field, can be successfully applied to (a) quantitatively explaining the experimentally observed prolate-to-oblate shape transition in the kHz region, and (b) more generally, to the experimentally obtained morphological phase diagram of GUVs with respect to two parameters, the frequency of the applied AC electric field, and the ratio of the electrical conductivities of the aqueous media inside and outside the vesicle [18]. The obtained results are compared with the findings in the literature, and the limitations of the model concerning the quantitative prediction of membrane deformation are discussed. Finally, an application of the observed effects in the conductometry of microliter samples is proposed.

**Acknowledgements** The author would like to thank Prof. S. Svetina and Prof. B. Žekš for numerous helpful discussions and V. Arrigler for the help with vesicle preparation. This work has been supported by the Slovenian Research Agency through grant J3-2268.

## References

1. Polk, C., Postow, E. (eds.): Handbook of biological effects of electromagnetic fields, 2nd edn. CRC Press, Boca Raton, New York, London, Tokyo (1996)
2. Zimmermann, U., Neil, G.A. (eds.): Electromanipulation of Cells. CRC Press, Boca Raton (1996)
3. Jones, T.B.: Electromechanics of particles. Cambridge University Press, Cambridge, New York, Melbourne (1995)
4. Zimmerman, U., Friedrich, U., Mussauer, H., Gessner, P., Hämel, K., Sukhorukov, V.: Electromanipulation of mammalian cells: Fundamentals and application. *IEEE Trans Plasma Sci* **28**, 72–82 (2000)
5. Gimsa, J.: A comprehensive approach to electro-orientation, electrodeformation, dielectrophoresis, and electrorotation of ellipsoidal particles and biological cells. *Bioelectrochemistry* **54**(1), 23–31 (2001)
6. Dimova, R., Riske, K.A., Aranda, S., Bezlyepkina, N., Knorr, R.L., Lipowsky, R.: Giant vesicles in electric fields. *Soft Matter* **3**, 817–827 (2007)
7. Dimova, R., Bezlyepkina, N., Domange Jordö, M., Knorr, R.L., Riske, K.A., Staykova, M., Vlahovska, P.M., Yamamoto, T., Yang, P., Lipowsky, R.: Vesicles in electric fields: some novel aspects of membrane behavior. *Soft Matter* **5**, 3201–3212 (2009)
8. Schwan, H.P.: Electrical properties of tissue and cell suspensions. *Adv. Biol. Med. Phys.* **5**, 147–209 (1957)
9. Helfrich, W.: Elastic properties of lipid bilayers: Theory and possible experiments. *Z. Naturforsch. C* **28**, 693–703 (1973)



10. Helfrich, W.: Deformation of lipid bilayer spheres by electric fields. *Z. Naturforsch. C* **29**, 182–183 (1974)
11. Bryant, G., Wolfe, J.: Electromechanical stresses produced in the plasma membranes of suspended cells by applied electric fields. *J. Membrane Biol.* **96**, 129–139 (1987)
12. Winterhalter, M., Helfrich, W.: Deformation of spherical vesicles by electric field. *J. Colloid Interf. Sci.* **122**, 583–586 (1988)
13. Harbich, W., Helfrich, W.: Alignment and opening of giant lecithin vesicles by electric fields. *Z. Naturforsch. A* **34**, 1063–1065 (1979)
14. Mitov, M.D., Méléard, P., Winterhalter, M., Angelova, M.I., Bothorel, P.: Electric-field-dependent thermal fluctuations of giant vesicles. *Phys. Rev. E* **48**(1), 628–631 (1993)
15. Peterlin, P., Svetina, S., Žekš, B.: The frequency dependence of phospholipid vesicle shapes in an external electric field. *Pflügers Arch. Eur. J. Physiol.* **439**, R139–R140 (2000)
16. Hyuga, H., Kinoshita Jr., K., Wakabayashi, N.: Transient and steady-state deformations of a vesicle with an insulating membrane in response to step-function or alternating electric fields. *Jpn. J. Appl. Phys.* **30**(10), 2649–2656 (1991)
17. Hyuga, H., Kinoshita Jr., K., Wakabayashi, N.: Steady-state deformation of a vesicle in alternating electric fields. *Bioelectrochem. Bioenerg.* **32**, 15–25 (1993)
18. Aranda, S., Riske, K.A., Lipowsky, R., Dimova, R.: Morphological transitions of vesicles induced by AC electric fields. *Biophys. J.* **95**, L19–L21 (2008)
19. Landau, L.D., Lifshitz, E.M., Pitaevskii, L.P.: *Electrodynamics of Continuous Media, Course of Theoretical Physics*, vol. 8, 2nd edn. Butterworth-Heinemann, Oxford (1984)
20. Nörtemann, K., Hilland, J., Kaatz, U.: Dielectric properties of aqueous NaCl solutions at microwave frequencies. *J. Phys. Chem. A* **101**, 6864–6869 (1997)
21. Turcu, I., Lucaciu, C.M.: Dielectrophoresis: a spherical shell model. *J. Phys. A: Math. Gen.* **22**, 985–993 (1989)
22. Foster, K.R., Sauer, F.A., Schwan, H.P.: Electrorotation and levitation of cells and colloidal particles. *Biophys. J.* **63**(1), 180–190 (1992)
23. Angelova, M.I., Dimitrov, D.S.: Liposome electroformation. *Faraday Discuss. Chem. Soc.* **81**, 303–311 (1986)
24. Angelova, M.I., Soléau, S., Méléard, P., Faucon, J.F., Bothorel, P.: Preparation of giant vesicles by external AC electric fields. Kinetics and applications. *Prog. Colloid Polym. Sci.* **89**, 127–131 (1992)
25. Peterlin, P., Arrigler, V.: Electroformation in a flow chamber with solution exchange as a means of preparation of flaccid giant vesicles. *Colloid. Surface. B* **64**, 77–87 (2008)
26. Sevšek, F., Sukharev, S., Svetina, S., Žekš, B.: The shapes of phospholipid vesicles in electric field as determined by video microscopy. *Stud. Biophys.* **138**, 143–146 (1990)
27. Sukhorukov, V.L., Meedt, G., Kürschner, M., Zimmerman, U.: A single-shell model for biological cells extended to account for the dielectric anisotropy of the plasma membrane. *J. Electrostat.* **50**, 191–204 (2001)
28. Ambjörnsson, T., Mukhopadhyay, G.: Dipolar response of an ellipsoidal particle with an anisotropic coating. *J. Phys. A: Math. Gen.* **36**, 10,651–10,665 (2003)
29. Ko, Y.T.C., Huang, J.P., Yu, K.W.: The dielectric behaviour of single-shell spherical cells with a dielectric anisotropy in the shell. *J. Phys.: Condens. Matter* **16**, 499–509 (2004)
30. Simeonova, M., Gimsa, J.: Dielectric anisotropy, volume potential anomalies and the persistent Maxwellian equivalent body. *J. Phys.: Condens. Matter* **17**, 7817–7831 (2005)
31. Peterlin, P., Svetina, S., Žekš, B.: The prolate-to-oblate shape transition of phospholipid vesicles in response to frequency variation of an AC electric field can be explained by the dielectric anisotropy of a phospholipid bilayer. *J. Phys.: Condens. Matter* **19**, 136220 (2007)
32. Vlahovska, P.M., Serral Gracià, R., Aranda-Espinoza, S., Dimova, R.: Electrohydrodynamic model of vesicle deformation in alternating electric field. *Biophys. J.* **96**, 4789–4803 (2009)
33. Kummrow, M., Helfrich, W.: Deformation of giant lipid vesicles by electric fields. *Phys. Rev. A* **44**(12), 8356–8360 (1991)
34. Niggemann, G., Kummrow, M., Helfrich, W.: The bending rigidity of phosphatidylcholine bilayers: Dependences on experimental method, sample cell sealing and temperature. *J. Phys. II France* **5**, 413–425 (1995)
35. Pott, T., Bouvrais, H., Méléard, P.: Giant unilamellar vesicle formation under physiologically relevant conditions. *Chem. Phys. Lipids* **154**, 115–119 (2008)
36. Horger, K.S., Estes, D.J., Capone, R., Mayer, M.: Films of agarose enable rapid formation of giant liposomes in solutions of physiologic ionic strength. *J. Am. Chem. Soc.* **131**, 1810–1819 (2009)